AIAA JOURNAL
Vol. 37, No. 1, January 1999

Inviscid Spatial Stability of a Developing Supersonic Axisymmetric Mixing Layer

Yung-Che Fang* and Eli Reshotko†
Case Western Reserve University, Cleveland, Ohio 44106

The instability characteristics of a developing supersonic axisymmetric mixing layer, with basic velocity profiles having wake components, is investigated numerically using linear inviscid stability theory in spatial formulation. The basic flow profiles are obtained by numerical solution of the compressible boundary-layer equations. For small convective Mach numbers, there are two unstable modes (the shear-layer and wake modes). If the convective Mach number is large enough, there are three unstable modes (the fast, slow, and wake modes). The slow mode consists of several similar modes, perhaps due to the axisymmetric geometry. It is also found that there is a mode-interchange phenomenon between the fast and slow modes and within the slow modes when the velocity profile has a wake component. Finally, the ratio between the streamwise and azimuthal wavelengths of the most amplified wave is almost constant. The normalized growth rate and the propagation angle of the most amplified wave are consistent with previous plane mixing layer results.

Nomenclature

C_{ph} = phase velocity of disturbance wave
M = Mach number
M^+ = convective Mach number, $M_1(1-\bar{U}_2)/(1+\sqrt{\bar{T}_2})$
m = azimuthal wave number
Pr = Prandtl number
p, $\bar{P}$ = pressure and mean pressure
Q = variable, $(\alpha^2+m^2/r^2)\bar{T}-M_1^2(\alpha\bar{U}-\omega)^2$
R = radius of the splitter plate
Re_1 = unit Reynolds number, $\bar{U}_1^*\bar{\rho}_1^*/\bar{\mu}_1^*$
R_α = normalized growth rate
r = radial coordinate
S = parameter of the Sutherland viscosity law, $110.6\,\mathrm{K}/\bar{T}_1^*$
$\bar{T}$ = mean temperature
$\bar{T}_w$ = wall temperature
t = time
$\bar{U}$, $\bar{V}$ = mean streamwise and transverse (radial) velocities
$\hat{U}$, $\hat{V}$ = transformed streamwise and transverse (radial) velocities
x = streamwise coordinate
x_{bl} = distance from the leading edge of flat plate
y = transverse coordinate, $r-R$
α = wave number in the streamwise direction
γ = specific heat ratio
η = transformed transverse coordinate
θ = propagation angle
θ_0 = total initial momentum thickness, $\theta_{0,1}+\theta_{0,2}$
λ_x, λ_χ = wavelength in the streamwise and azimuthal directions
$\bar{\mu}$ = mean viscosity
ξ = transformed streamwise coordinate
Π = amplitude of pressure disturbances
$\bar{\rho}$ = mean density
χ = azimuthal coordinate
ω = temporal frequency

Subscripts

i = imaginary part
interface = quantity at the interface
r = real part
1, 2 = quantity at the jet and external freestreams

Superscript

$*$ = dimensional quantity

Received June 16, 1997; revision received Aug. 10, 1998; accepted for publication Aug. 10, 1998. Copyright © 1998 by the American Institute of Aeronautics and Astronautics, Inc. All rights reserved.

*Graduate Research Assistant, Department of Mechanical and Aerospace Engineering.
†Kent H. Smith Professor of Engineering, Department of Mechanical and Aerospace Engineering. Fellow AIAA.

Introduction

KNOWLEDGE of the instability characteristics of compressible mixing layers is of fundamental importance. It may benefit the understanding of noise generation mechanisms or the enhancing of air/fuel mixing inside the combustion chamber of modern aircraft jet engines. There are a lot of investigations of compressible mixing layers. For example, Jackson and Grosch[1] studied the spatial stability of compressible plane mixing layers. At low Mach number, there is only a single unstable mode. A second unstable mode appears if the Mach number exceeds a critical value. One of these two unstable modes is the fast mode with high phase velocity, and the other is the slow mode with low phase velocity. It was also shown that oblique (three-dimensional) disturbances have similar behavior to two-dimensional disturbances but with higher growth rate at some propagation angles, and the maximum growth rate occurs for oblique disturbances. Liang[2] also confirms the appearance of two unstable modes in a supersonic plane mixing layer for both spatial and temporal stability formulations.

In the initial region of the mixing layer, the velocity profile always has a wake component because boundary layers exist on both sides of the splitter plate. Koochesfahani and Frieler[3] studied the linear spatial stability of an incompressible plane wake/mixing layer. Two unstable modes are found. One is the shear-layer mode, whose corresponding unstable waves lead to the usual Kelvin–Helmholtz shear layer roll-up pattern, and the other is the wake mode.

For compressible flow, Liang et al.[4] carried out a numerical calculation of spatial stability for an unbounded developing mixing layer formed by two supersonic streams and showed that there are three unstable modes, which are fast, slow, and very slow modes. The slowest mode is the wake mode. The other two modes correspond to the fast and slow modes of the self-similar mixing layer.[1] Similarly, Zhuang and Dimotakis[5] found two unstable modes in the spatial stability of a supersonic developing mixing layer for low Mach corresponding to the shear-layer and wake modes for the incompressible developing mixing layer.[3] With increasing Mach number, the shear-layer mode splits into fast and slow modes and the wake mode remains unsplit. The two-dimensional mode is the most unstable mode if the basic velocity profile has a relatively strong wake component. Conversely, the three-dimensional mode is the most unstable mode in the case of a small wake component.

The object of the present work is to numerically study the instability pattern of a developing supersonic axisymmetric mixing layer by linearized inviscid stability theory. The wake-like structure of the basic flow is solved numerically, based on the boundary-layer approximation. Studies are performed at several downstream locations, which cover the range from near the splitter plate to beyond the point where the wake component disappears. The number of unstable modes for the developing mixing layer is determined by a global spectral method. The effect of the azimuthal wave number on the linear instability for the developing mixing layer is also studied.

Formulation of the Problem

The basic flow profiles are calculated by considering a mixing layer formed by two parallel compressible laminar boundary layers over an axisymmetric splitter. Each flow is uniform outside its boundary layer at the trailing edge and is assumed to be nonreacting and subject to the perfect gas law. Because of the presence of boundary layers at the splitter, the mixing layer exhibits a wake-like structure beyond the trailing edge. At some distance downstream of the trailing edge, the viscous forces smooth out the wake-like profile, and eventually the velocity profile becomes monotonic.

Flow variables are nondimensionalized by the following definitions:

$$(x, r, y, R) = \frac{(x^*, r^*, y^*, R^*)}{\left(\theta_0^{*2} Re_1, \theta_0^*, \theta_0^*, \theta_0^*\right)}$$

$$(\bar{U}, \bar{V}, \bar{P}) = \frac{(\bar{U}^*, \bar{V}^*, \bar{P}^*)}{\left(\bar{U}_1^*, \bar{U}_1^*/Re_1\theta_0^*, \bar{\rho}_1^*\bar{U}_1^{*2}\right)} \tag{1}$$

$$(\bar{\rho}, \bar{T}, \bar{\mu}) = \frac{(\bar{\rho}^*, \bar{T}^*, \bar{\mu}^*)}{\left(\bar{\rho}_1^*, \bar{T}_1^*, \bar{\mu}_1^*\right)}$$

The dimensionless governing equations for the mixing layers are given by

$$\frac{\partial}{\partial x}(r\bar{\rho}\bar{U}) + \frac{\partial}{\partial y}(r\bar{\rho}\bar{V}) = 0 \tag{2}$$

$$\bar{\rho}\bar{U}\frac{\partial \bar{U}}{\partial x} + \bar{\rho}\bar{V}\frac{\partial \bar{U}}{\partial y} = \frac{1}{r}\frac{\partial}{\partial y}\left(r\bar{\mu}\frac{\partial \bar{U}}{\partial y}\right) \tag{3}$$

$$\bar{\rho}\bar{U}\frac{\partial \bar{T}}{\partial x} + \bar{\rho}\bar{V}\frac{\partial \bar{T}}{\partial y} = \frac{1}{Pr}\frac{1}{r}\frac{\partial}{\partial y}\left(r\bar{\mu}\frac{\partial \bar{T}}{\partial y}\right) + (\gamma - 1)M_1^2\bar{\mu}\left(\frac{\partial \bar{U}}{\partial y}\right)^2 \tag{4}$$

$$\bar{\rho}\bar{T} = 1 \tag{5}$$

Both γ and Pr are assumed constant. The viscosity coefficient obeys the Sutherland viscosity law $\bar{\mu} = \bar{T}^{3/2}(1 + S)/(\bar{T} + S)$. The initial and boundary conditions are

$$\begin{aligned} &\bar{U} = \bar{U}(y), && \bar{T} = \bar{T}(y) && \text{for} && x = 0 \\ &\bar{U} = \bar{U}_2, && \bar{T} = \bar{T}_2 && \text{for} && r \to \infty \\ &\bar{U} = 1, && \bar{T} = 1, && \bar{V} = 0 && \text{for} && r = 0 \end{aligned} \tag{6}$$

Note that velocity at the centerline equals the jet freestream velocity assuming it is still in the core.

Equations (2–5) are discretized by a fully implicit marching finite difference scheme in the timelike streamwise direction and a multidomain spectral collocation method in the transverse direction.[6] At each marching station, the coupled spectral discretization equations are solved by the preconditioned Richardson iteration method to a specified level of accuracy.

For simplicity, the initial profiles at the splitter trailing edge are assumed to be the similarity solutions of a two-dimensional boundary-layer flow. This assumes that $\theta_0^*/R^* \ll 1$. The governing equations for a two-dimensional boundary-layer flow are similar to Eqs. (2–5) except that the radius factors are discarded. A coordinate transformation[7] is introduced to allow easy transfer from boundary-layer coordinates to mixing-layer coordinates:

$$\xi = \sqrt{2x_{\text{bl}}}, \qquad \eta = \frac{y}{\sqrt{2x_{\text{bl}}}}, \qquad \hat{U} = \bar{\rho}\bar{U}, \qquad \hat{V} = \bar{\rho}(\xi\bar{V} - \eta\bar{U}) \tag{7}$$

The resulting dimensionless governing equations are given by

$$\hat{U} + \frac{\partial \hat{V}}{\partial \eta} = 0 \tag{8}$$

$$\hat{V}\frac{\partial \bar{U}}{\partial \eta} = \frac{\partial}{\partial \eta}\left(\bar{\mu}\frac{\partial \bar{U}}{\partial \eta}\right) \tag{9}$$

$$\hat{V}\frac{\partial \bar{T}}{\partial \eta} = \frac{1}{Pr}\frac{\partial}{\partial \eta}\left(\bar{\mu}\frac{\partial \bar{T}}{\partial \eta}\right) + (\gamma - 1)M_1^2\bar{\mu}\left(\frac{\partial \bar{U}}{\partial \eta}\right)^2 \tag{10}$$

The initial boundary-layer profiles at the trailing edge are solved individually for the external flow and the jet. The boundary conditions for the external flow are

$$\begin{aligned} &\bar{U} = \bar{U}_2, && \bar{T} = \bar{T}_2 && \text{for} && \eta \to +\infty \\ &\bar{U} = \hat{V} = 0, && \bar{T} = \bar{T}_w && \text{for} && \eta = 0 \end{aligned} \tag{11}$$

and for the jet are

$$\begin{aligned} &\bar{U} = \hat{V} = 0, && \bar{T} = \bar{T}_w && \text{for} && \eta = 0 \\ &\bar{U} = 1, && \bar{T} = 1 && \text{for} && \eta \to -\infty \end{aligned} \tag{12}$$

The wall temperature $\bar{T}_w$ equals the average of jet and external total temperatures. Equations (8–10) are also solved by the multidomain spectral collocation method.

Linear stability analysis is done by imposing an infinitesimal disturbance on the basic flow and observing it over space and time. This slight disturbance will not interact with other disturbances or the basic flow, and nonlinear terms in the stability equations can be discarded. The time-dependent quantities can be considered in the form of a superposition of mean flow quantities and infinitesimal fluctuation terms. The basic flow is assumed a locally parallel flow, and axial gradients of basic flow quantities are neglected. Based on the normal-mode analysis, the disturbance term can be Fourier decomposed. For example, the time-dependent pressure is given by $p = \bar{P} + \Pi(r)\exp[i(\alpha x + m\chi - \omega t)]$. Other flow quantities have a similar form. The flow quantities for the stability analysis are nondimensionalized by θ_0^*, $\bar{U}_1^*$, $\theta_0^*/\bar{U}_1^*$, $\bar{\rho}_1^*$, $\bar{T}_1^*$, and $\bar{\rho}_1^*\bar{U}_1^{*2}$ for length, velocities, time, density, temperature, and pressure, respectively.

Substituting the decomposed forms into the governing equations and neglecting viscous and conductive terms, the linearized inviscid stability equations become[6]

$$\frac{\mathrm{d}^2\Pi}{\mathrm{d}r^2} - \left(\frac{2\alpha}{\alpha\bar{U} - \omega}\frac{\mathrm{d}\bar{U}}{\mathrm{d}r} - \frac{1}{\bar{T}}\frac{\mathrm{d}\bar{T}}{\mathrm{d}r} - \frac{1}{r}\right)\frac{\mathrm{d}\Pi}{\mathrm{d}r} - \frac{Q}{\bar{T}}\Pi = 0 \tag{13}$$

and the boundary conditions are

$$\begin{aligned} &\Pi \to 0 && \text{or bounded at } r = 0 \\ &\Pi \to 0 && \text{at } r \to \infty \end{aligned} \tag{14}$$

The linearized inviscid stability equation (13) is solved by a hybrid method, i.e., using the global method (Chebyshev spectral collocation method) to compute all of the eigenvalues first, and applying the local method (Runge–Kutta shooting method) to refine particular eigenvalues and to compute the corresponding eigenfunctions.[6]

Results

A single-subdomain spectral method is applied to both the jet and external stream boundary-layer calculations at the trailing edge. A two-subdomain spectral method is applied to the following downstream mixing-layer calculation where one subdomain covers the region of $y \geq 0$ and the other one $y \leq 0$.

The present results are obtained for three sets of parameters, as shown in Table 1. Parameters are taken at sea level for a jet engine and external static temperature is equal to 294 K. Primarily, the effect of jet Mach number is investigated, i.e., $M_1 = 1.4$, 1.8, and 2.2. For all three cases, $\bar{U}_2 = 0.25$, $\bar{T}_2 = 0.5$, $Pr = 0.72$, $\gamma = 1.4$, $S = 0.188$, $R = 100$, and $\theta_{0,1} = \theta_{0,2}$. The values of M_1 are chosen so that M^+ covers the range from 0.6 to 1.0.

Table 1 Computational parameters

Parameters	Case 1	Case 2	Case 3
M_1	1.4	1.8	2.2
M_2	0.495	0.636	0.778
M^+	0.615	0.791	0.967

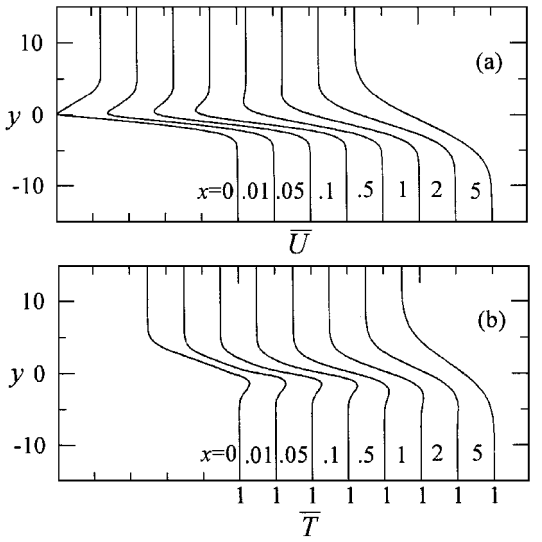

Fig. 1 Profiles of basic flow for $M_1 = 1.4$: a) velocity and b) temperature.

The coordinate parameters for the initial boundary-layer calculations at the trailing edge are $\eta_{\text{interface}} = 0, -20$ for the jet and $\eta_{\text{interface}} = 0, 20$ for the external stream. For the downstream mixing-layer calculation, those are $y_{\text{interface}} = -20, 0, 20$. To resolve the rapid-change basic profile, more collocation points are required near the region of $y = 0$. The convergence criterion is that the maximum pointwise velocity and temperature errors between two consecutive iterations are less than a specified tolerance of 10^{-10}. Each subdomain has 101 collocation points. The marching step Δx is equal to 10^{-4} for $0 \le x \le 0.1$ and gradually expanded to 10^{-2} by 10% at each step for $0.1 < x \le 5$. The basic profiles at each station possess at least five-digit accuracy. Figure 1 shows the velocity and temperature profiles for $M_1 = 1.4$ at various streamwise locations. The other two cases, $M_1 = 1.8$ and 2.2, have similar profiles. The wake-like character of the velocity profiles disappears by $x = 1$ for all three cases, and the jet core persists to the end of the computational domain.

Instability characteristics of the first 26 azimuthal wave numbers ($0 \le m \le 25$) for $M_1 = 1.4$ are all resolved. Results for only four azimuthal wave numbers ($m = 0$, 5, 15, and 25) are plotted in Figs. 2 and 3. There are two unstable modes (the shear-layer and wake modes). The wake mode disappears when the velocity profile has no wake component at $x \ge 1$ and is consistent with previous plane wake/mixing layer calculations.[3–5] The shear-layer mode is more unstable than the wake mode at all streamwise locations. As m increases, both the shear-layer and wake modes become less unstable. However, in Ref. 3 it was found that at some flow conditions the shear-layer mode is more unstable and at other flow conditions the wake mode is more unstable.

The maximum growth rates for the first 26 azimuthal wave numbers are plotted in Fig. 4. At the initial mixing-layer region ($x = 0.01$–0.5), the maximum growth rates of the first 26 azimuthal wave numbers are nearly equal. Farther downstream, the growth rates of the higher azimuthal wave numbers begin to diminish. For example, at $x = 5$ only the first 15 azimuthal wave numbers remain amplified. This trend is similar to the jet stability calculation at farther downstream locations.[8] The most amplified waves for $M_1 = 1.4$ correspond to the axisymmetric shear-layer mode at all streamwise locations.

Results of linear instability for $M_1 = 1.8$ are shown in Figs. 5 and 6. The two unstable modes are the same as those for $M_1 = 1.4$. The

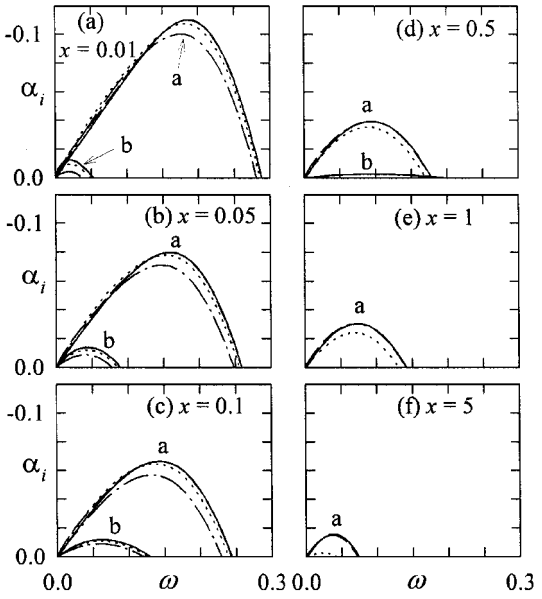

Fig. 2 Variation of spatial growth rate vs frequency for $M_1 = 1.4$: ——, $m = 0$; – – –, $m = 5$; - - - -, $m = 15$; and – – –, $m = 25$; a is shear-layer mode, and b is wake mode.

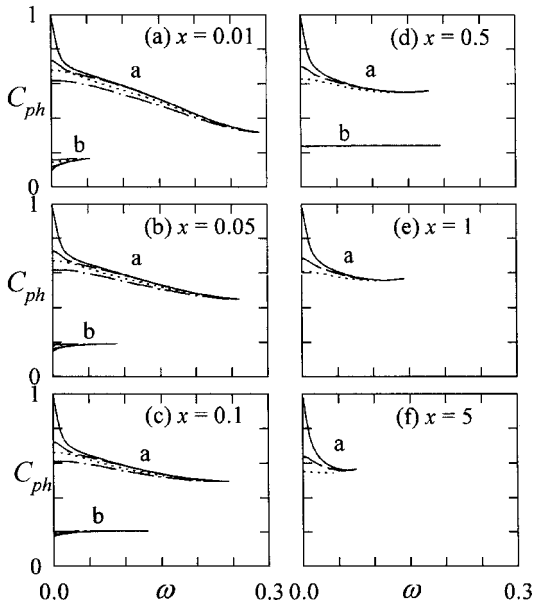

Fig. 3 Variation of phase velocity vs frequency for $M_1 = 1.4$: ——, $m = 0$; – – –, $m = 5$; - - - -, $m = 15$; and – – –, $m = 25$; a is shear-layer mode, and b is wake mode.

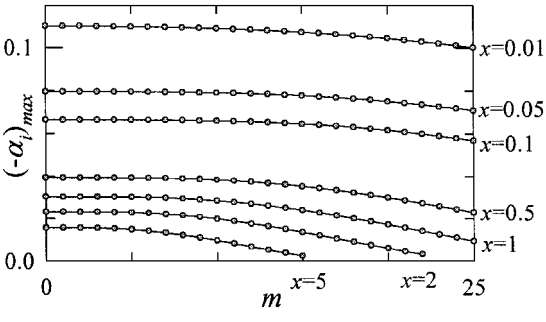

Fig. 4 Spatial growth rate of the most amplified wave as a function of azimuthal number for $M_1 = 1.4$.

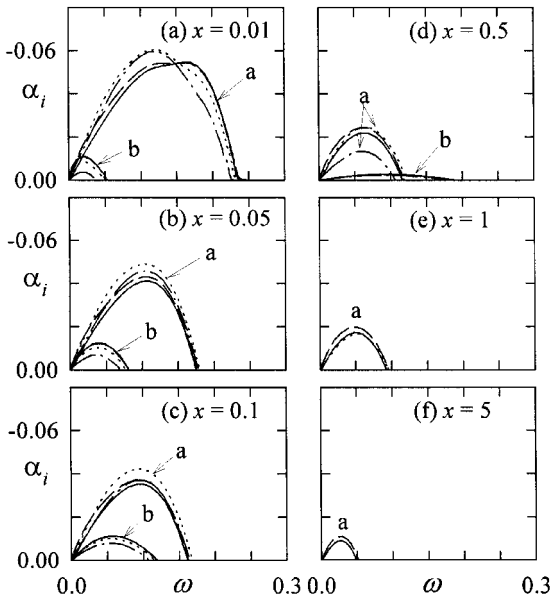

Fig. 5 Variation of spatial growth rate vs frequency for $M_1 = 1.8$: ——, $m = 0$; – – –, $m = 5$; - - - -, $m = 15$; and – - –, $m = 25$; a is shear-layer mode, and b is wake mode.

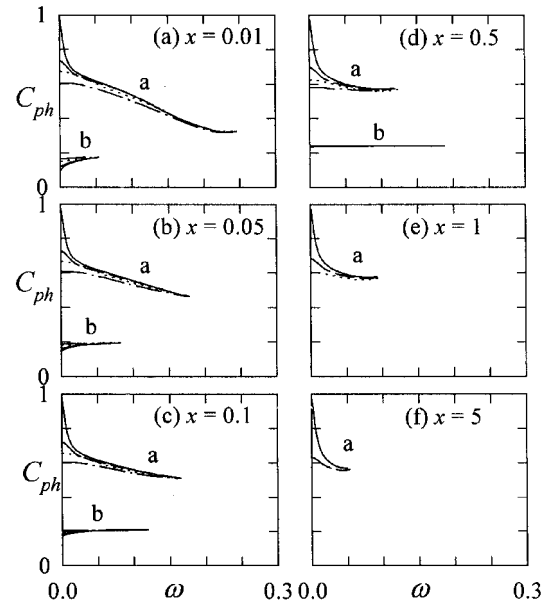

Fig. 6 Variation of phase velocity vs frequency for $M_1 = 1.8$: ——, $m = 0$; – – –, $m = 5$; - - - -, $m = 15$; and – - –, $m = 25$; a is shear-layer mode, and b is wake mode.

shear-layer mode is also more unstable than the wake mode. The maximum growth rates for the first 26 azimuthal wave numbers are plotted in Fig. 7. It is found that the most amplified wave corresponds to the azimuthal shear-layer mode instead of the axisymmetric mode, which is different than that for $M_1 = 1.4$. As x increases, the most amplified wave has lower azimuthal wave number. For example, the most amplified wave number is $m = 19$ at $x = 0.01$ and $m = 4$ at $x = 5$.

The growth rate as a function of frequency for axisymmetric modes ($m = 0$) at $M_1 = 2.2$ is shown in Fig. 8. There are three unstable modes because the shear-layer mode splits into two modes and the wake mode stays unsplit when M_1 changes from 1.8 to 2.2. The two shear-layer modes are classified as the fast and slow modes, where the fast mode always has higher phase velocity than the slow mode (cf. Fig. 9). The mode-splitting result is consistent with plane mixing layer instability calculations.[1,5] The slow modes actually consist of several distinct modes with similar instability characteristics. Most of the slow modes are distributed at high frequencies

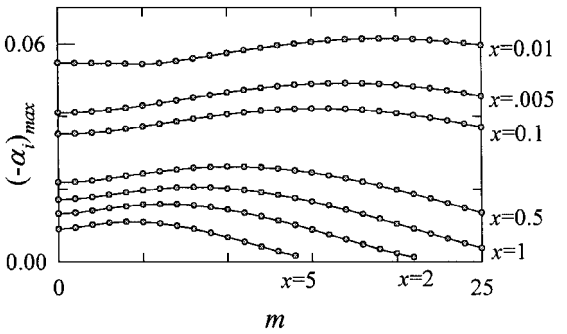

Fig. 7 Spatial growth rate of the most amplified wave as a function of azimuthal wave number for $M_1 = 1.8$.

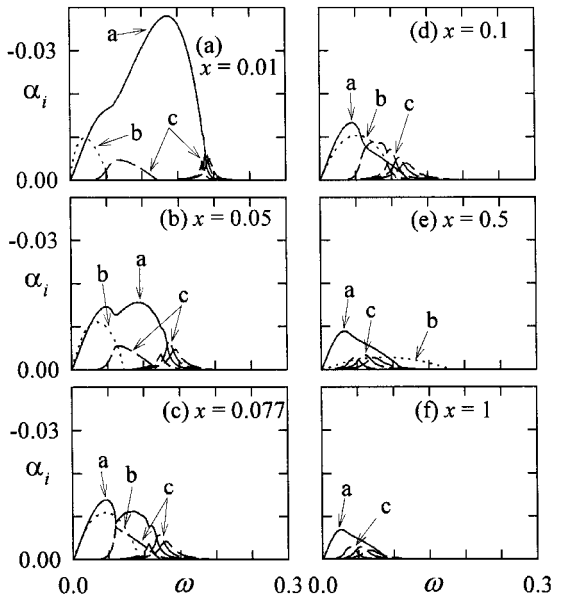

Fig. 8 Variation of spatial growth rate vs frequency for $m = 0$ and $M_1 = 2.2$; a is fast mode, b is wake mode, and c is slow mode.

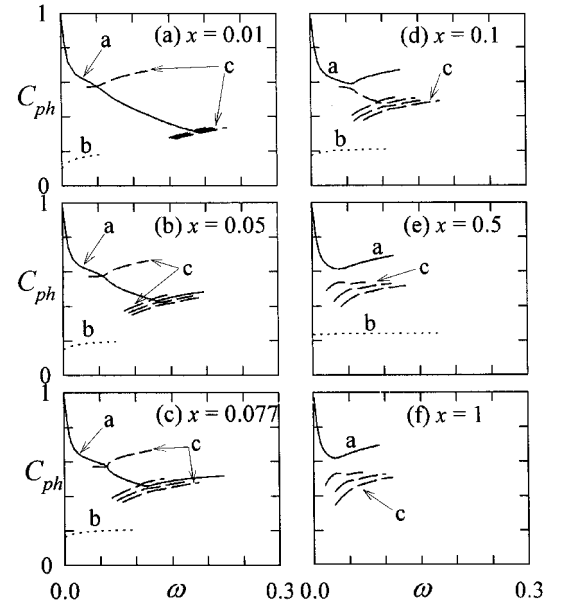

Fig. 9 Variation of phase velocity vs frequency for $m = 0$ and $M_1 = 2.2$; a is fast mode, b is wake mode, and c is slow mode.

near the neutral instability point of the fast mode. Only a few of the slow modes with the largest growth rates are shown in Figs. 8 and 9.

The fast mode is always more unstable than the slow and wake modes at all streamwise locations. This is contrary to Ref. 4, in which the wake mode (slow mode II in their terminology) is dominant in the initial downstream region. Farther downstream, the wake mode becomes stable, and the fast mode becomes the dominant mode thereafter. A similar calculation on a plane wake/mixing layer[5] has shown that the slow mode emerges as the dominant mode for two-dimensional disturbances, also contrary to the present result.

Figure 9 shows the variation of the phase velocity with the frequency for $m = 0$ and $M_1 = 2.2$. A mode-interchange phenomenon between the fast and slow modes is found for $x < 0.1$, where the basic velocity profile has a strong wake component. For $x < 0.1$, the phase velocity curve of the fast mode always cuts through those of the slow mode and this cut-through feature of the phase velocity curves actually corresponds to a mode interchange between the fast and slow modes. Referring to Fig. 8, as the mixing layer moves farther downstream from $x = 0.01$, the growth rate of the fast mode at higher frequencies decreases faster than that at lower frequencies. At the same time, a single slow mode at middle frequencies keeps growing. Eventually at a certain downstream location (see Fig. 8c for $x = 0.077$), the higher frequency portion of the fast mode degenerates to a new slow mode, and the original slow mode emerges as a part of the fast mode. The mode interchange between the fast and slow modes occurs not only at middle frequencies but also at high frequencies, whereas the interchanging at middle frequencies affects the growth rate more than that at high frequencies.

At $x = 0.1$, the mode interchange between the fast and slow modes is diminished. Only a single curve of the slow mode cuts through other curves of the slow mode, and this corresponds to the mode interchange within the slow modes (cf. Fig. 9d). For $x \geq 0.5$, there is no further mode interchange, and the fast and slow modes behave independently. In the mode-interchange region, what is fast and what is slow are not always obvious. The present classifications reflect the nature of these modes downstream of the mode-interchange region, which is in the later mixing layer region.

The emergence of several slow modes for the developing axisymmetric mixing layer probably originates from the axisymmetric geometry. For the higher azimuthal wave numbers ($m > 0$), the instability characteristics are similar to the axisymmetric mode except there is no slow mode at the middle frequency and only distributed in the high-frequency region. This suggests that the mode interchange between the fast and slow modes occurs only at high frequencies for the higher azimuthal wave numbers. The instability characteristics of the fast mode are plotted in Figs. 10 and 11, and the results for four azimuthal wave numbers are shown. Generally speaking, they

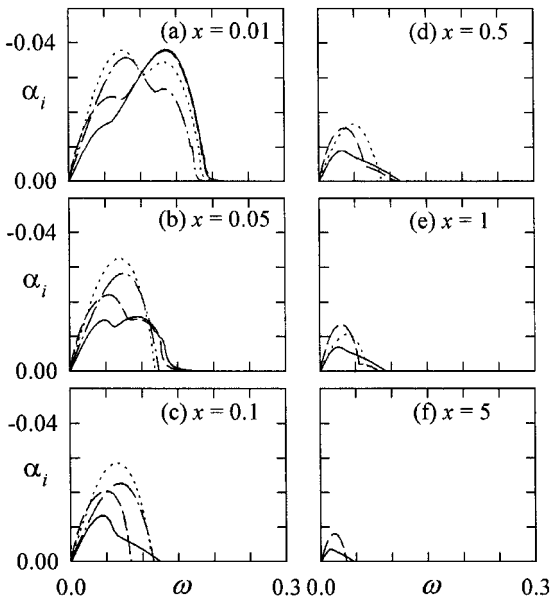

Fig. 10 Variation of spatial growth rate of the fast mode vs frequency for $M_1 = 2.2$: ——, $m = 0$; – – –, $m = 5$; - - - -, $m = 15$; and – - –, $m = 25$.

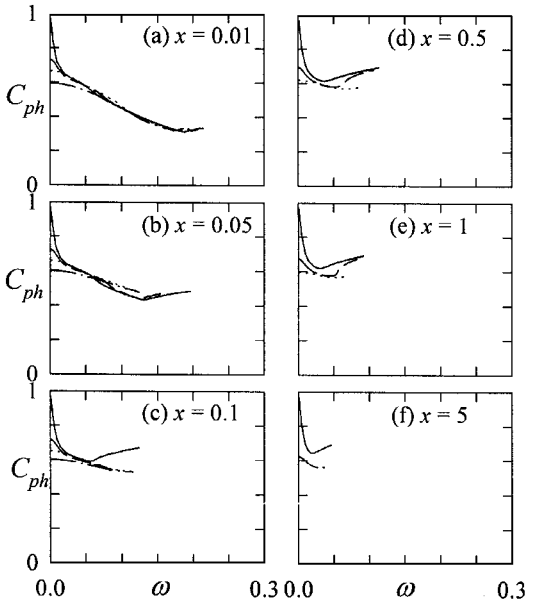

Fig. 11 Variation of phase velocity of the fast mode vs frequency for $M_1 = 2.2$: ——, $m = 0$; – – –, $m = 5$; - - - -, $m = 15$; and – - –, $m = 25$.

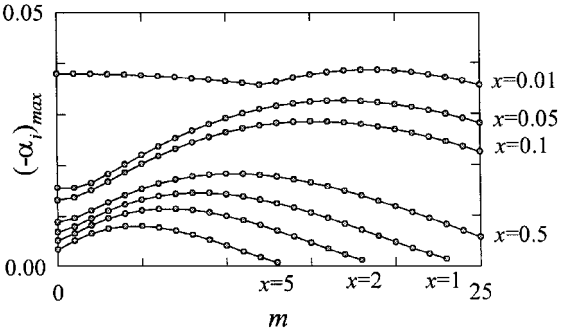

Fig. 12 Spatial growth rate of the most amplified wave as a function of azimuthal number for $M_1 = 2.2$.

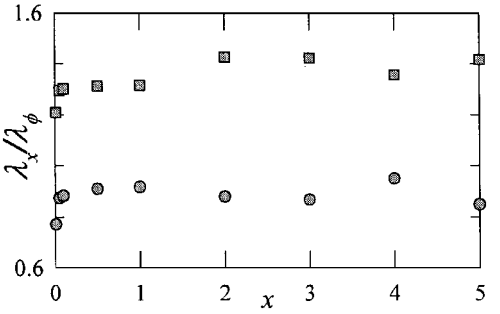

Fig. 13 Variation of ratio of streamwise wavelength to azimuthal wavelength vs streamwise coordinate for various M_1; ▩ is $M_1 = 1.8$, and ▨ is $M_1 = 2.2$.

are similar to those for $M_1 = 1.8$ (Figs. 5 and 6). Figure 12 shows the maximum growth rates for the first 26 azimuthal wave numbers. At $x = 0.01$, the maximum growth rates of the first 26 azimuthal wave numbers ($0 \leq m \leq 25$) are nearly equal. As x increases, the most amplified wave has lower azimuthal wave number, which is similar to that for $M_1 = 1.8$. For example, the most amplified wave number is $m = 17$ at $x = 0.05$ and $m = 5$ at $x = 5$.

The ratio between the streamwise and azimuthal wavelengths for the most amplified waves is

$$\lambda_x / \lambda_\chi = m / \alpha_r R \tag{15}$$

The ratio λ_x / λ_χ of the most amplified azimuthal waves is shown in Fig. 13 only for those at $M_1 = 1.8$ and 2.2 because the most amplified wave occurs for the axisymmetric mode at $M_1 = 1.4$. The ratios

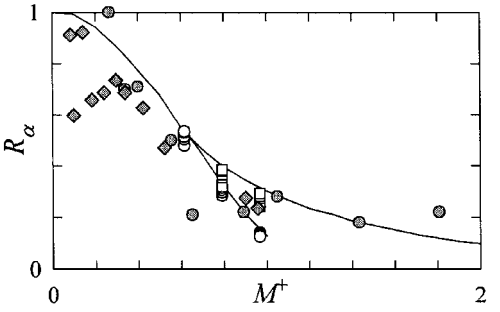

Fig. 14 Variation of normalized growth rate vs convective Mach number: ○, present two-dimensional waves; □, present azimuthal waves; ◍, Ref. 10; ——, two-dimensional waves of Ref. 9; – – –, oblique waves of Ref. 9; and ◈, Ref. 11.

λ_x/λ_χ for $M_1 = 1.8$ and 2.2 at most streamwise locations ($x \geq 0.05$) are almost constant at values of 0.89 and 1.36, respectively. This suggests that the azimuthal waves in a developing mixing layer evolve in such a way that the ratio between the streamwise and azimuthal wavelengths is nearly constant.

The average propagation angle $\theta = \tan^{-1} m/\alpha_r R$ for $M_1 = 1.8$ ($M^+ = 0.791$) is 41.7 deg, and for $M_1 = 2.2$ ($M^+ = 0.967$) it is 53.7 deg. These values are similar to those of plane mixing layers because the propagation angles for plane mixing layers at $M^+ = 0.8$ and 1 are 46.8 and 56.2 deg, respectively.[9]

The present results are compared with those for plane mixing layers by considering the variation of growth rate with convective Mach number. To make the comparison, a normalized growth rate is introduced:

$$R_\alpha = \frac{\left[-\alpha_i\left(M^+, m, \bar{U}_2, \bar{T}_2\right)\right]_{\text{most amplified}}}{\left[-\alpha_i\left(M^+ = 0, m = 0, \bar{U}_2, \bar{T}_2\right)\right]_{\text{most amplified}}} \qquad (16)$$

where the maximum growth rate is scaled by its incompressible two-dimensional counterpart.[10] The present results together with those of previous plane mixing layer investigations[9–11] are shown in Fig. 14. The present normalized growth rates are taken at streamwise locations $x = 0.01, 0.05, 0.1, 0.5, 1, 2,$ and 5 for $M^+ = 0.615, 0.791,$ and 0.967. It is shown that R_α of the most amplified waves for all three cases $M^+ = 0.615, 0.791,$ and 0.967 is nearly constant at most investigated streamwise locations ($x \geq 0.05$). For a plane mixing layer, when $M^+ < 0.64$, the most amplified wave is a two-dimensional wave. As M^+ increases, the azimuthal disturbance becomes more unstable than the two-dimensional wave. The present results are consistent with those of Ragab and Wu.[9] It is clearly shown that the growth rate behavior of an axisymmetric compressible mixing layer in the early developing region is similar to that of a plane mixing layer.

Concluding Remarks

The instability of a compressible axisymmetric mixing layer is studied using inviscid stability theory. It is shown that wake-like basic flow profiles and axisymmetric geometry affect the instability characteristics significantly. One of the unstable modes, the wake mode, only occurs for wake-like basic flow profiles. Emergence of several slow modes probably originates from the axisymmetric geometry. These slow modes will give a new degree of complexity to problems where the slow modes dominate. In these circumstances, the nonlinearity between these slow modes cannot be neglected. Also, the mode-interchange phenomenon that appears at the highest convective Mach number of this investigation is quite interesting and requires further study.

Acknowledgments

The authors express their gratitude to the Ohio Supercomputer Center for using the Cray Y-MP8/864 supercomputer through Grant PDS130-3. The authors wish to acknowledge helpful discussions with Ernst W. Mayer and Fang-Pei Liang and also want to thank F.-P. Liang for the use of his numerical code in the early stage of the present work.

References

[1] Jackson, T. L., and Grosch, C. E., "Inviscid Spatial Stability of a Compressible Mixing Layer," *Journal of Fluid Mechanics*, Vol. 208, 1989, pp. 609–637.

[2] Liang, F.-P., "An Inviscid Stability Analysis of Unbounded Supersonic Mixing Layer Flows," Ph.D. Dissertation, Dept. of Mechanical and Aerospace Engineering, Case Western Reserve Univ., Cleveland, OH, Jan. 1991.

[3] Koochesfahani, M. M., and Frieler, C. E., "Instability of Nonuniform Density Free Shear Layers with a Wake Profile," *AIAA Journal*, Vol. 27, No. 12, 1989, pp. 1735–1740.

[4] Liang, F.-P., Reshotko, E., and Demetriades, A., "A Stability Study of the Developing Mixing Layer Formed by Two Supersonic Laminar Streams," *Physics of Fluids*, Vol. 8, Dec. 1996, pp. 3253–3263.

[5] Zhuang, M., and Dimotakis, P. E., "Instability of Wake-Dominated Compressible Mixing Layers," *Physics of Fluids*, Vol. 7, Oct. 1995, pp. 2489–2495.

[6] Fang, Y.-C., "Inviscid Spatial Stability of an Axisymmetric Compressible Developing Mixing Layer," Ph.D. Dissertation, Dept. of Mechanical and Aerospace Engineering, Case Western Reserve Univ., Cleveland, OH, Jan. 1997.

[7] Pruett, C. D., and Streett, C. L., "A Spectral Collocation Method for Compressible, Non-Similar Boundary Layers," *International Journal for Numerical Methods in Fluids*, Vol. 13, Nos. 5–6, 1991, pp. 713–737.

[8] Cohen, J., and Wygnanski, I., "The Evolution of Instabilities in the Axisymmetric Jet, Part 1: The Linear Growth of Disturbances near the Nozzle," *Journal of Fluid Mechanics*, Vol. 176, 1987, pp. 191–219.

[9] Ragab, S. A., and Wu, J. L., "Linear Instabilities in Two-Dimensional Compressible Mixing Layers," *Physics of Fluids A*, Vol. 1, June 1989, pp. 957–966.

[10] Papamoschou, D., and Roshko, A., "The Compressible Turbulent Shear Layer: An Experimental Study," *Journal of Fluid Mechanics*, Vol. 197, 1988, pp. 453–477.

[11] Hall, J. E., Dimotakis, P. E., and Rosemann, H., "Experiments in Nonreacting Compressible Shear Layers," *AIAA Journal*, Vol. 31, No. 12, 1993, pp. 2247–2254.

G. M. Faeth
Editor-in-Chief